Journal of Materials Science & Technology 76 (2021) 111–121

Contents lists available at ScienceDirect

Journal of Materials Science & Technology

journal homepage: www.jmst.org

Research Article

Negative thermal expansion in one-dimension of a new double sulfate $AgHo(SO_4)_2$ with isolated SO_4 tetrahedra

Yuriy G. Denisenko[a,b,c], Victor V. Atuchin[d,e,f,*], Maxim S. Molokeev[g,h,i], Naizheng Wang[j], Xingxing Jiang[j], Aleksandr S. Aleksandrovsky[k,l], Alexander S. Krylov[m], Aleksandr S. Oreshonkov[h,m], Alexander E. Sedykh[b,n], Svetlana S. Volkova[a], Zheshuai Lin[j,o], Oleg V. Andreev[a,p], Klaus Müller-Buschbaum[b,n]

[a] Institute of Chemistry, Tyumen State University, Tyumen, 625003, Russia
[b] Institute of Inorganic and Analytical Chemistry, Justus-Liebig-University of Giessen, 35392, Giessen, Germany
[c] Department of General and Special Chemistry, Industrial University of Tyumen, Tyumen, 625000, Russia
[d] Laboratory of Optical Materials and Structures, Institute of Semiconductor Physics, SB RAS, Novosibirsk, 630090, Russia
[e] Laboratory of Semiconductor and Dielectric Materials, Novosibirsk State University, Novosibirsk, 630090, Russia
[f] Research and Development Department, Kemerovo State University, Kemerovo, 650000, Russia
[g] Laboratory of Crystal Physics, Kirensky Institute of Physics, Federal Research Center KSC SB RAS, Krasnoyarsk, 660036, Russia
[h] Siberian Federal University, Krasnoyarsk, 660041, Russia
[i] Department of Physics, Far Eastern State Transport University, Khabarovsk, 680021, Russia
[j] Technical Institute of Physics and Chemistry, Chinese Academy of Sciences, Beijing, 100190, China
[k] Laboratory of Coherent Optics, Kirensky Institute of Physics, Federal Research Center KSC SB RAS, Krasnoyarsk, 660036, Russia
[l] Institute of Nanotechnology, Spectroscopy and Quantum Chemistry, Siberian Federal University, Krasnoyarsk, 660041, Russia
[m] Laboratory of Molecular Spectroscopy, Kirensky Institute of Physics, Federal Research Center KSC SB RAS, Krasnoyarsk, 660036, Russia
[n] Center for Materials Research (LaMa), Justus-Liebig-University Giessen, Giessen, 35392, Germany
[o] University of the Chinese Academy of Sciences, Beijing, 100049, China
[p] Laboratory of the Chemistry of Rare Earth Compounds, Institute of Solid State Chemistry, UB RAS, Ekaterinburg, 620137, Russia

ARTICLE INFO

Article history:
Received 26 June 2020
Received in revised form 3 August 2020
Accepted 15 August 2020
Available online 27 October 2020

Keywords:
Sulfate
Crystal structure
Thermal expansion
Raman
Photoluminescence
Band structure

ABSTRACT

A double holmium-silver sulfate was obtained for the first time. The temperature intervals for the formation and stability of the compound were determined by differential scanning calorimetry. The crystal structure of $AgHo(SO_4)_2$ was determined by Rietveld method. The X-ray diffraction (XRD) analysis showed that the compound crystallizes in the monoclinic syngony, space group $P2_1/m$, with the unit cell parameters $a = 4.71751$ (4) Å, $b = 6.84940$ (6) Å and $c = 9.89528$ (9) Å, $\beta = 95.1466$ (4)°, $V = 318.448$ (5) Å^3, $Z = 2$, $R_B = 1.55$ %, $T = 303$ K. Two types of sulfate tetrahedra were found in the structure, which significantly affected the spectral properties in the infrared range. In the temperature range of 143–703 K, a negative thermal expansion along the b direction accompanied by a positive thermal expansion along the a and c directions was observed. It was established that negative thermal expansion is the result of the deformation of sulfate tetrahedra, which is affected by the movement of holmium and silver atoms. The excitation in the blue spectral range (457.9 nm) produces a luminescence in light blue (489 nm), green (545 nm) and red (654 nm) spectral ranges, and the latter two were of comparable intensity that is favorable for WLED sources. The observed luminescent band distribution is ascribed to the specific crystal field at Ho^{3+} ion sites rather than a variation of radiationless probability.

1. Introduction

The exploration of the basic relationships between the structure of solids and their chemical and physical properties is one of the most important tasks in materials science, since understanding these relationships is necessary to obtain materials with specified properties [1–4]. The relationships can be revealed by

* Corresponding author at: Laboratory of Optical Materials and Structures, Institute of Semiconductor Physics, SB RAS, Novosibirsk, 630090, Russia.
E-mail address: atuchin@isp.nsc.ru (V.V. Atuchin).

https://doi.org/10.1016/j.jmst.2020.10.026
1005-0302/

a comparative analysis of experimental and theoretical results reported for different crystals and crystal families. In this connection, the less studied and new materials are of particular interest because it is possible to see new and unexpected effects on their structural behavior and physical characteristics. Such materials evidently include complex sulfate crystals containing rare earth elements although the permanent research activity flowed in this and closely related fields over the recent years [5–15]. Among binary anhydrous sulfates, the $AgLn(SO_4)_2$ (Ln = rare earth elements) family is known [12,16]. However, up to now, only one compound $AgEu(SO_4)_2$ has been characterized by structural and spectroscopic methods [12]. Besides, the fragmentary report on the unit cell parameters of $AgPr(SO_4)_2$ and $AgEr(SO_4)_2$ sulfates was found in the literature [16]. The triclinic structures in space group *P*-1 were found in all three compounds $AgLn(SO_4)_2$ (Ln = Pr, Eu, Er), but additionally, the existence of the monoclinic modification in space group $P2_1/m$ was reported for $AgEr(SO_4)_2$ [16]. This information can be considered as an indicator of the rich crystal chemistry of binary sulfates $AgLn(SO_4)_2$ for the case of heavy rare earth elements. The structural instability can be assumed, including a possible phase transition between monoclinic and triclinic modifications. To test this hypothesis, the present study is aimed at the synthesis of binary sulfate $AgHo(SO_4)_2$ and the evaluation of its properties by experimental and theoretical methods.

The selection of holmium for the experiment is specified by the spectroscopic parameters of Ho^{3+} ions in oxide hosts. Among the rare-earth elements, Ho^{3+} ions, due to their appropriate metastable states, have interesting luminescence parameters for optical applications in visible and infrared spectral ranges. The radiation of Ho^{3+}-based lasers lies in the range of 1.2–4.9 mm, and the lasers are most promising in several biomedical applications [17–23]. The doping of Ho^{3+} ions, in combination with Yb^{3+}, Eu^{3+} or Er^{3+}, to oxide crystal hosts is widely applied for the creation of up-conversion luminescent materials with multicolor light generation [24–28]. In the present study, $AgHo(SO_4)_2$ was prepared in the powder form via the solid state reaction similar to the algorithm previously designed for $AgEu(SO_4)_2$ [12]. Then, the structural, thermal and spectroscopic characterizations were implemented by conventional experimental methods. The electronic structure of $AgHo(SO_4)_2$ was investigated by ab initio theoretical methods.

2. Experimental methods

Double holmium-silver sulfate was synthesized by the solid-phase interaction between simple sulfates according to reaction:

$$Ag_2SO_4 + Ho_2(SO_4)_3 \rightarrow 2AgHo(SO_4)_2 \quad (1)$$

Reagents of the highest available degree of purity were used in the synthesis: Ho_2O_3 (99.99 %, ultrapure, TDM-96 Ltd., Russia), concentrated nitric acid ($C(HNO_3)$ =14.6 mol L^{-1}, ultrapure, Vekton Ltd., Russia), concentrated sulfuric acid ($C(H_2SO_4)$ =17.9 mol L^{-1}, ultrapure, Vekton Ltd., Russia). First, holmium sulfate was prepared in accordance with the following reactions:

$$Ho_2O_3 + 6HNO_3 \rightarrow 2Ho(NO_3)_3 + 3H_2O \quad (2)$$

$$2Ho(NO_3)_3 + 3H_2SO_4 \rightarrow Ho_2(SO_4)_3\downarrow + 6HNO_3 \quad (3)$$

5.0 g of holmium oxide was weighed on an analytical balance (ME-204, MettlerTolledo, Switzerland) and transferred to a 100 mL round bottom flask. Then, 5 mL of bidistilled deionized water was added to the Ho_2O_3 powder. Then, 6.5 mL of concentrated nitric acid was added to the suspension. Strong overheating of the reaction mixture should not be allowed. The result of this manipulation is a transparent and slightly yellow solution of holmium nitrate. If the solution is cloudy, it should be slightly heated until the solid particles of oxide are completely dissolved.

Then, 2.6 mL (excess 10 %) of concentrated sulfuric acid is carefully added to the transparent solution with a vigorous stirring. The result of the reaction is a light yellow precipitate of holmium sulfate. The resulting reaction mixture was distilled off with a direct refrigerator to a dry residue. The distillation is neutralized with a weak alkaline solution and disposed of as saline. The dry residue is calcined in a quartz reactor at the temperature of 500 °C for 7 days to remove adsorbed acids and obtain the high-crystallinity sulfate $Ho_2(SO_4)_3$. The $Ho_2(SO_4)_3$ powder should be stored in a tightly closed container, preferably in a desiccator above sulfuric acid or phosphorus pentoxide, to prevent occasional hydration. At all stages of working with acid solutions, it is strictly forbidden to use metal instruments. The acid volume measurement was carried out using glass graduated pipettes only. Spatulas, tweezers and other supplies should be made of thermostable plastics. When working with concentrated acid solutions, the general safety requirements for working in a chemical laboratory should be strictly followed.

For the synthesis of $AgHo(SO_4)_2$, Ag_2SO_4 and $Ho_2(SO_4)_3$ were taken as starting reagents. The dry reagents were weighed according to the nominal composition on an analytical balance at the accuracy of 0.1 mg. The main difficulty in the complex sulfate synthesis is avoiding the occasional hydration of the reagents due to their high affinity to water vapor in the laboratory air. In the weighing room, it is recommended to maintain humidity at a lower limit specified in the technical documentation of the corresponding analytical balance, but not less than 30 %.

The stoichiometric mixture of Ag_2SO_4 and $Ho_2(SO_4)_3$ was ground in an agate mortar for 1 h. After that, the resulted batch was quantitatively transferred to an alumina crucible and calcined in a muffle furnace at 923 K for 12 h in the air. After cooling it to 303 K, the obtained cake was ground in an agate mortar for 1 h and the annealing process was repeated for 12 h. The resulted product, like all silver salts, should be stored in a dark glass packaging and in a dark place to avoid the photochemical destruction. As a final product, a dense cake is formed, and it can hardly be rubbed off. As shown in Fig. S1 (in Supporting Information), the sample is pale yellow, the characteristic color of the oxide compounds containing Ho^{3+} ions.

The powder X-ray diff ;raction (XRD) data of $AgHo(SO_4)_2$ for the structural analysis were collected at temperatures 303, 503 and 703 K with a Bruker D8 ADVANCE powder diff ;ractometer (Cu-*K*α radiation) using an Anton Paar heat attachment and linear VANTEC detector. The 2θ range of 10°-144° was measured with a 0.6 mm divergence slit, the step size of 2θ was 0.016° and the counting time was 1.5 s per step. Additional 15 XRD patterns were measured in the temperature range of 143−703 K. In this case, the 2θ range of 8°-90° was measured with the 0.6 mm divergence slit, the step size of 2θ was 0.016° and the counting time was 0.4 s per step. The particle morphology observation by scanning electron microscopy (SEM) and chemical composition determination by energy dispersive spectroscopy (EDS) were carried out using a Tescan MIRA3 LMU SEM with an Oxford Instruments Ultim Max 65 attachment at electron energy of 20 kV. To accumulate and process the spectra, the Oxford Instruments AZtec software was used. Due to the semiconductor nature of the sample, the deposition of conductive coatings was not required.

The thermal analysis was carried out in the Ar flow at a simultaneous thermal analysis (STA) equipment 499 F5 Jupiter NETZSCH (Germany). The powder samples were inserted into alumina crucibles. The heating rate was 5 °C min^{-1}. For the enthalpy determination, the equipment was initially calibrated with the standard metal substances, such as In, Sn, Bi, Zn, Al, Ag, Au and Ni. The heat effect peaks were evaluated with the package «Proteus 6 2012». The peak temperatures and areas in parallel experiments were reproduced at an inaccuracy lower than 0.3 %.

The Fourier-transform infrared spectroscopy (FTIR) measurements were carried out using a Fourier transform infrared spectrometer FSM 1201. The sample for the investigation was prepared as a tablet with adding the annealed KBr. The luminescence and Raman spectra of $AgHo(SO_4)_2$ at room temperature were recorded by a Horiba Jobin-Yvon T64000 spectrophotometer with a nitrogen cooled charge-coupled device (CCD) camera in subtractive dispersion mode. The Spectra-Physics Stabilite 2017 Ar^+ ion laser was used as an excitation light source. The 457.9 nm line with the power of 5 mW on the sample was used for recording luminescence spectra. The CCD pixel coverage was as fine as 0.004 nm at 670 nm and 0.01 nm at 450 nm. The radiation with λ =514.5 nm and the 5 mW power on the sample was used to record the Raman spectra.

Temperature measurements of the luminescence were performed by a Horiba Jobin Yvon Spex Fluorolog 3 spectrophotometer equipped with a 450 W Xe short-arc lamp (USHIO), double-grating excitation and emission monochromators, and a photomultiplier tube (R928 P), using a FluoroEscence software. The sample was placed into a quartz glass cuvette, and spectra were recorded at room temperature and at 77 K (using special liquid nitrogen-filled Dewar assembly). Both excitation and emission spectra were corrected for the spectral response of the monochromators and that of the detector using spectra corrections provided by the manufacturer. In addition, excitation spectra were corrected for the spectral distribution of the lamp intensity by using a photodiode reference detector.

3. Computation methods

The first-principles spin-polarized electronic structure calculation of $AgHo(SO_4)_2$ was performed by the CASTEP package [29], a total energy package based on the plane-wave pseudopotential density functional theory (DFT) [30,31]. In the present calculations, the unit cell parameters and positions of the constituent atoms of $AgHo(SO_4)_2$, as obtained by Rietveld analysis, were initially optimized and then were used in band structure calculations. The Perdew-Burke-Emzerhof (PBE) [32] function within the generalized gradient approximation (GGA) [33] was chosen to describe the exchange-correlation function. The effective interaction between the atomic cores and valence electrons were modeled by optimized norm-conserving pseudopotentials [34]. In this model, Ag $4p^6 4d^{10} 5s^1$, Ho $4f^{11} 5s^2 5p^6 5d^\circ 6s^2$, S $3s^2 3p^6$ and O $2s^2 2p^6$ are treated as valence electrons. Such calculation parameters can allow a small plane-wave basis set while ensuring the calculation accuracy. The kinetic energy cutoff of 550 eV and the intensive Monkhorst-Pack [35] k-point meshes spanning less than 0.07 $Å^{-3}$ were chosen. Furthermore, the GGA + U [36] method with the on-site orbital dependent Hubbard U energy term U_f =5 eV [37] for the Ho $4f$ orbital was employed to consider the effect of localized f-orbitals in transition elements. To ensure the computational accuracy for vibrational properties, the convergence tolerance and q-vector grid spacing were set to 10^{-7} eV $Å^{-2}$ and 0.07 $Å^{-1}$, respectively. The convergence test showed that the calculation result is less than the allowable error and the above computational parameters are accurate enough for the purposes of this study. Using the DFT calculation, the vibration modes of $AgHo(SO_4)_2$ at different wavenumbers are simulated and they are shown in Supporting Information file. To investigate the effect of temperature on lattice vibration, the phonon density of states was calculated and the weighing factor under Boltzmann distribution, $e^{-}(\hbar w/K_B T)$, was weighed into the phonon density of states.

4. Results and discussion

The profile fitting, crystal structure searching and Rietveld refinements were performed by using TOPAS 4.2 [38]. All reflections of the $AgHo(SO_4)_2$ compound at T = 303 K were indexed by primitive monoclinic cell (a = 4.712 Å, b = 6.843 Å, c = 9.888 Å, β = 95.12°, V = 317.67 $Å^3$, GoF = 43.0), and the analysis of reflection extinction showed that the most probable space group is $P2_1/m$ or $P2_1$. The highest symmetry $P2_1/m$ group was chosen as an initial model. The crystal structure was solved using a simulated annealing procedure applied to the randomized coordinates of one Ag^+ and one Ho^{3+} ions, and the randomized coordinates together with the orientation angles of two SO_4^{2-} tetrahedra [39]. The dynamical occupancy correction of the atoms was used to merge the ions falling in a special position [39,40]. After the calculations, a solution was found with small R-factors. The crystal structure contains one Ag^+ and one Ho^{3+} ions, and both are in the special position (2e) on mirror plane m. Two independent SO_4 tetrahedra are also located in special sites (2e) (Fig. 1(a)). The refinement of this model was stable and gave low R-factors (Table 1, Fig. 1(b)). The coordinates of atoms and main bond lengths are summarized in Tables S1 and S2 in Supporting Information, respectively. The structural analysis of $AgHo(SO_4)_2$ using the program PLATON [41] did not reveal any problems with the symmetry, bond lengths in the structure, and thus the $P21/m$ space group was chosen correctly. The absence of any empty voids proves that there are no any additional ions/molecules in the structure of compound. The crystallographic data of the crystal structures at 303, 503 and 703 K are deposited in Cambridge Crystallographic Data Centre (CSD # 434504, 434,544 and 434,545). The data can be downloaded from the site (www.ccdc.cam.ac.uk/data_request/cif).

The bond valence sum for Ho^{3+} using values r_0 = 1.992 Å, b_0 = 0.37 [42] and eight bond lengths d(Ho-O) in the range of (2.158 (9)- 2.73 (1) Å) gave the value BVS(Ho^{3+}) = 3.45, which is close to the 3+ valence state of Ho ions. As a result, we can suppose that the Ho^{3+} ions form square-antiprism HoO_8. Similar calculations for all S^{6+} ions using r_0 = 1.624 Å, b_0 = 0.37 [43] gave BVS(S1) = 4.70 and BVS(S2) = 5.92, which are also in agreement with the 6+ valence state (about +/−20 % of average value) of S ions. The HoO_8 polyhedron is coordinated by two chelately bonded SO_4 and four monodentately bonded SO_4 tetrahedra (Fig. 1(a)). The bond valence calculations made for the Ag^+ ion using parameters r_0 = 1.842 Å, b_0 = 0.37 [43] and only five bond lengths in the range of 2.296 (8)-2.880 (9) Å gave BVS(Ag^+) = 0.96, which is close to the 1+ valence state of Ag ions. Therefore, one can suggest the formation of AgO_5 polyhedron. The τ parameter for the coordination environment of Ag^+ was calculated using the procedure proposed by literature [44]. The obtained value (τ = 0.74) is considerably closer to the trigonal-bipyramid (ideally τ = 1) than to the square-pyramid (ideally τ = 0). It should be noted that there are three long distances d(Ag-O) in the range of 3.004 (7)-3.127 (9) Å, which could not be taken as bond lengths, but can be considered as short contacts Ag. . .O (Fig. 1(a)). Taking into account these contacts, one can get the AgO_8 polyhedron, which is similar to the HoO_8 polyhedron (Fig. 1(a)). In this work, the short contacts were not accounted, assuming trigonal prisms AgO_5. These prisms are joined with each other by nodes to form an infinity chain along the a-axis (Fig. 1(a)). Also, they are coordinated by one chelately bonded SO_4, three monodentately bonded SO_4 tetrahedra and three HoO_8 polyhedrons through O nodes. Totally, all structural elements form a 3D net. The topological analysis of the net in ToposPro program [45], using simplification that HoO_8, AgO_5, $S1O_4$, $S2O_4$ are nodes, revealed that this is a 4-nodal (4-c)(6-c)(9-c)(11-c) net with the point symbol $(3.4^5)(3^6.4^{20}.5^8.6^2)(3^6.4^9)(3^8.4^{20}.5^{15}.6^{12})$, which is new. It should be noted that, taking into account the AgO_8 polyhedron instead of AgO_5, one can get a simplified 2-nodal (6-c)(12-c) net with the point symbol $(3^{12}.4^{33}.5^{16}.6^5)(3^6.4^9)$, which is also new.

Heating the sample from 143 to 703 K leads to a decrease in cell parameter b and monoclinic angle β. Simultaneously, an increase in parameters a and c is observed (Table S3 in Supporting Information, Fig. 2). The related tensor of thermal expansion is shown

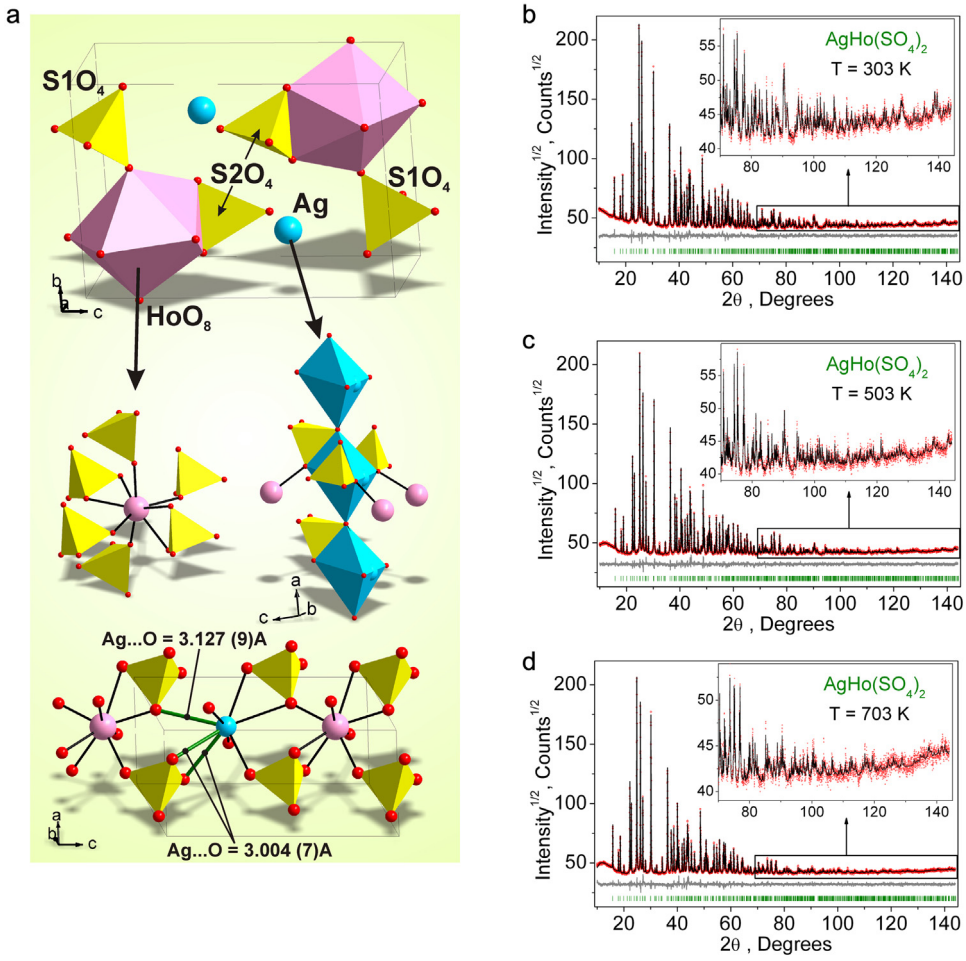

Fig. 1. (a) Crystal structure of $AgHo(SO_4)_2$ and different Rietveld plots at (b) $T = 303$, (c) $T = 503$ and (d) $T = 703$ K.

Table 1
Main parameters of processing and refinement of the sample $AgHo(SO_4)_2$.

T (K)	Space group	a (Å)	b (Å)	c (Å)	β (°)	V (Å^3)	Z	2θ-interval (°)	No. of reflections	No. of refined parameters	R_{wp} (%)	R_p (%)	R_{exp} (%)	χ^2	R_B (%)
303	$P2_1/m$	4.71751 (4)	6.84940 (6)	9.89528 (9)	95.1466 (4)	318.448 (5)	2	10–144	686	61	3.29	2.51	2.06	1.59	1.55
503	$P2_1/m$	4.75129 (4)	6.84223 (6)	9.93141 (9)	95.0258 (4)	321.623 (5)	2	10–144	693	61	3.51	2.62	2.17	1.62	1.56
703	$P2_1/m$	4.80158 (6)	6.83505 (8)	9.9648 (1)	94.8957 (5)	325.841 (7)	2	10–144	700	61	3.76	2.61	2.17	1.74	2.05

in Fig. 3. The tensor was plotted with the software PASCaL [46]. It is seen that the thermal expansion in $AgHo(SO_4)_2$ is strongly anisotropic and, just along the crystallographic axis b, the negative thermal expansion appears on heating (shown by blue color). In summary, the negative thermal expansion along the b-direction does not lead to a cell volume decrease and, therefore, the thermal expansion is ordinal (Fig. 2(e)). As far as Ag, Ho, O2, O3, O4 and O6 ions are located in the special 2e Wyckoff sites and lie in the mirror plane m, which is orthogonal to the b-axis, their movements under heating/cooling cannot lead to the changes of b-axis length. Contrary, O1 and O5 ions are in the general sites 4f and the negative thermal expansion along b should be associated with them. The detailed analysis of the variations of bond lengths $d(X\text{-O1})$, $d(X\text{-O5})$ and valence angles O1-X-O1, O5-X-O5, where X = Ag, Ho, S1, S2 (Fig. S2 in Supporting Information), reveals that the largest crystal structure distortion under heating/cooling is associated with the O1 ion, and the corresponding thermal expansion coefficients of geometric parameters under heating are: O1-Ag-O1 ($\alpha = -6.52 \times 10^{-7}$ K^{-1}); O1-Ho-O1 ($\alpha = -1.99 \times 10^{-7}$ K^{-1}); d(Ag–O1) ($\alpha = 2.02 \times 10^{-7}$ K^{-1}); d(Ho-O1) ($\alpha = 2.99 \times 10^{-7}$ K^{-1}); d(S1-O1) ($\alpha = -2.8 \times 10^{-7}$ K^{-1}) (Fig. S2(a), (c), (e), (g), and (i) in Supporting Information). Therefore, it is offered to estimate the b-axis length value from d(Ag-O1), d(Ho-O1), O1-Ag-O1 and O1-Ho-O1 values (Fig. 4). First of all, it was found that O1-S1-O1 and O5-S2-O5 angles are almost persistent under heating (Fig. S2(k) and (l)). Since the d(S1-O1) bond length decreases and angle O1-S-O1 does not change under heating, this means that the $b1$ projection of d(S1-O1) into the b-axis decreases under heating (Fig. 4). The $b2$ projection of d(Ho-O1) into the b-axis is equal to the product of increasing value d(Ho-O1) and decreasing value sin((O1-Ho-O1)/2), and, therefore, it should not have a prominent increasing/decreasing value. If so, the b-axis value is equal to the sum of decreasing value $b1$ and almost constant value $b2$, which gives the decreasing b value under heating (Fig. 4).

The nature of the motion of O1 ion can be explained by the increasing d(Ag-O1) together with d(Ho-O1) bond lengths, which push the O1 ion toward the S1 ion, decreasing the d(S1-O1) bond length. Another mechanism of decreasing the b-axis is associated with pushing the O5 ion by the Ho ion toward the Ag ion. The shifts

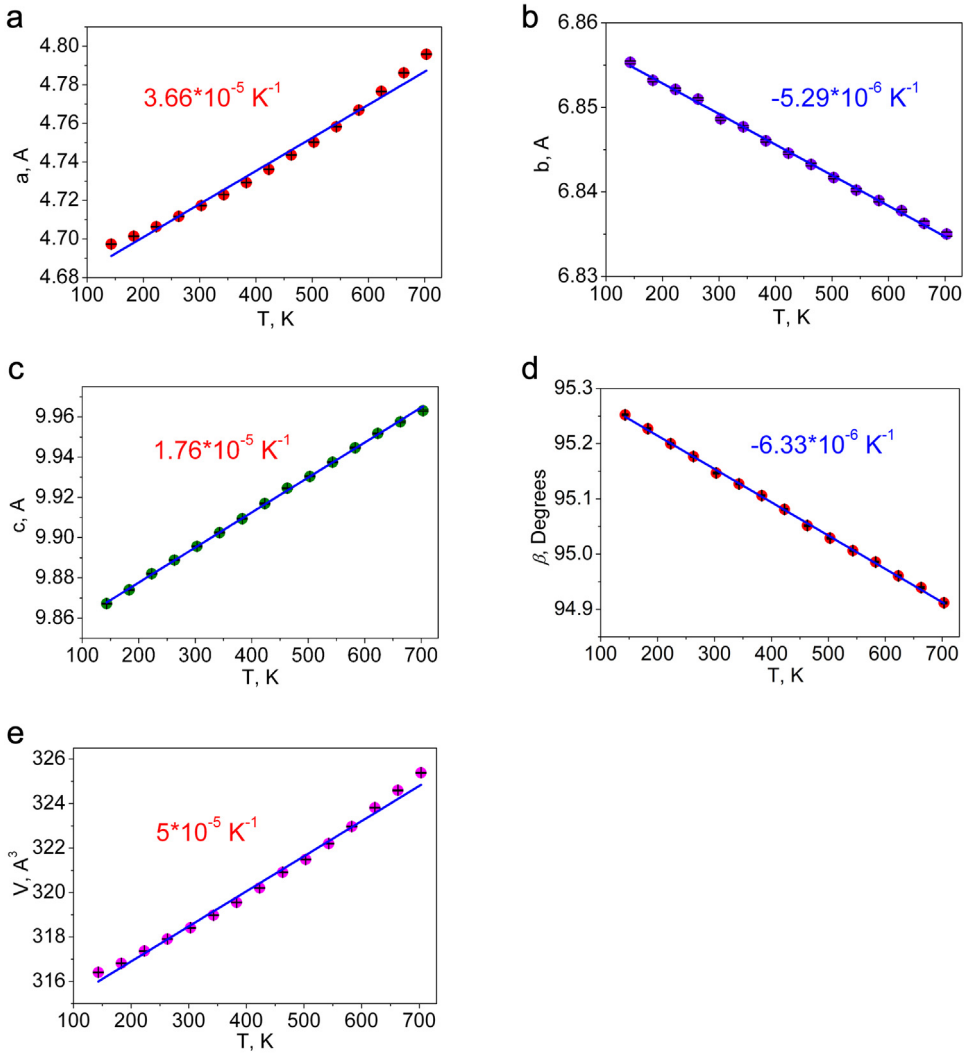

Fig. 2. Cell parameter dependences on temperature: (a) a (T), (b) b (T), (c) c (T), (d) β (T) and (e) V (T).

of these ions are not so prominent in comparison with that of the O1 ion, and, anyway, the calculation of b-axis from the equations:

$$b = 2\times d(\text{Ho-O1})\times\sin((\text{O1-Ho-O1})/2) + 2\times d(\text{S1-O1})\times\sin((\text{O1-S1-O1})/2) \quad (4)$$

$$b = 2\times d(\text{Ag-O5})\times\sin((\text{O5-Ag-O5})/2) + 2\times d(\text{S2-O5})\times\sin((\text{O5-S2-O5})/2) \quad (5)$$

gave the decrease of b value in both cases (Table S4 in Supporting Information).

The SEM image recorded for $AgHo(SO_4)_2$ is shown in Fig. 5. According to these data, the product obtained as a result of solid phase synthesis is mainly composed of dense particles with the size of 5–15 μm without any characteristic faceting. The results of the EDS measurements are listed in Table 2. Besides, one EDS spectrum measured for the $AgHo(SO_4)_2$ sample is shown in Fig. S3 (in Supporting Information). Only the strong signals of constituent elements are observed in the spectrum and these elements are accounted only in the calculations of chemical composition. As it is evident from Table 2, the excellent relationship is observed between measured and theoretical compositions. The constituent element distributions over the powder $AgHo(SO_4)_2$ sample are presented in Fig. 6. As it is seen, all four distributions are uniform. Generally, the EDS measurements confirm the formation of $AgHo(SO_4)_2$.

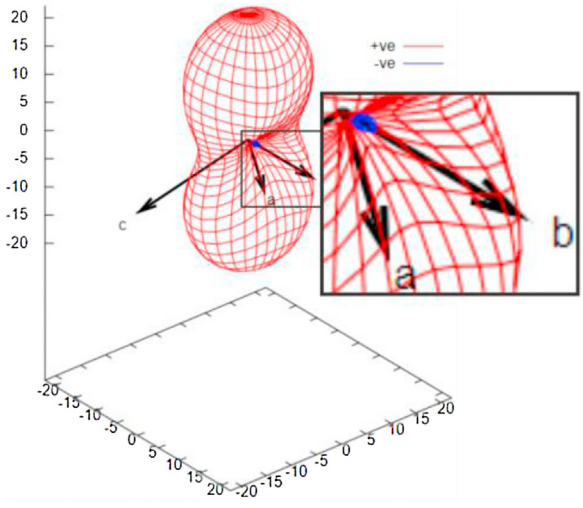

Fig. 3. Thermal expansion tensor of $AgHo(SO_4)_2$.

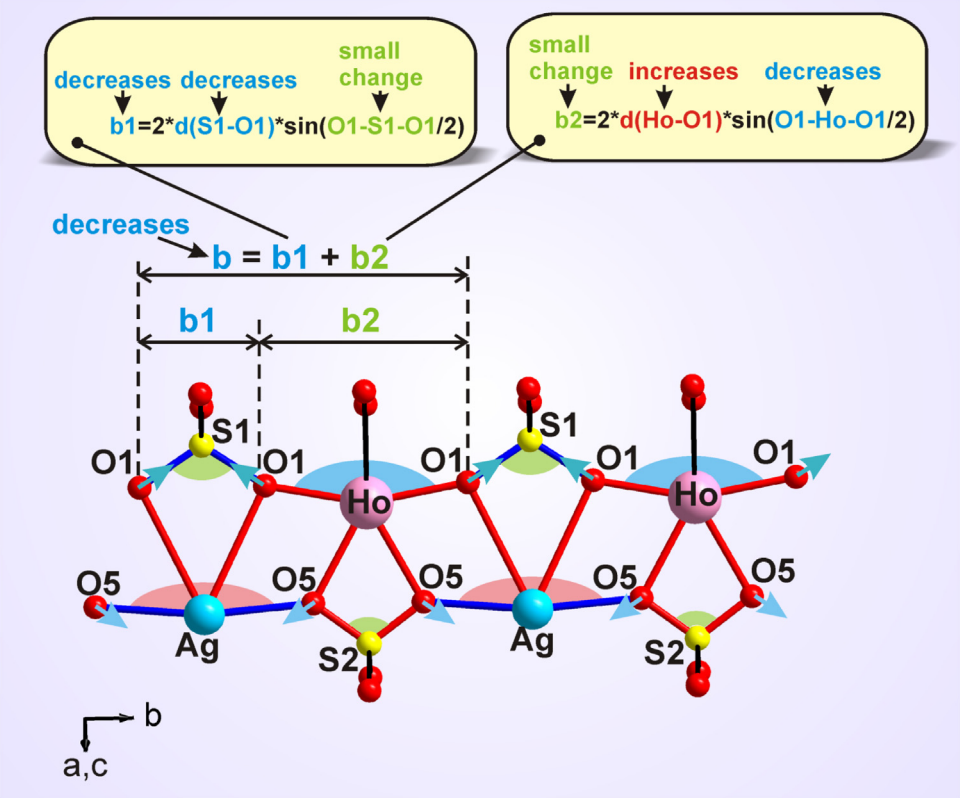

Fig. 4. Structure transformations appeared upon heating. The bonds, which increase on heating, are red and, contrary, the bonds, which decrease on heating, are blue. The bond angles, which increase, decrease and are unchanged under heating are marked by red, blue and green sectors, respectively. Blue short arrows indicate the O^{2-} ion move.

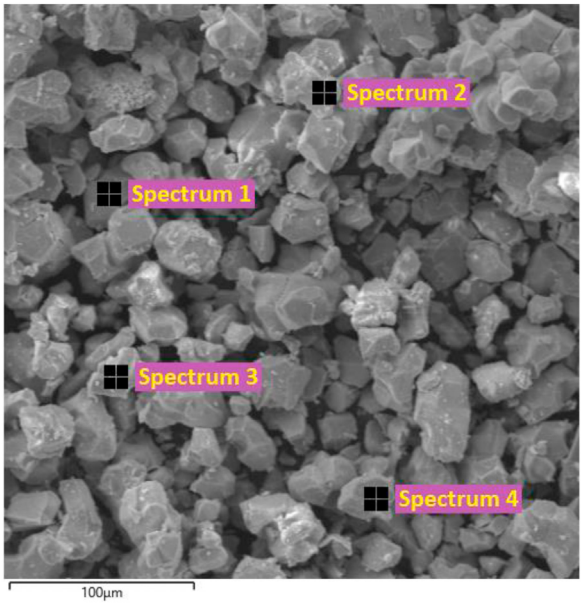

Fig. 5. SEM image of $AgHo(SO_4)_2$ particles. The fields used for EDS analysis are indicated.

To study the solid-phase interaction, the stoichiometric mixture of Ag_2SO_4 and $Ho_2(SO_4)_3$ sulfates was studied by differential scanning calorimetry and thermogravimetry. The obtained dependence is shown in Fig. 7. Peak A, which begins at 422.8 °C, corresponds to the polymorphous transformation of silver sulfate according to the literatures [47–50]:

$$\beta\text{-}Ag_2SO_{4(rhomb)} \rightarrow \alpha\text{-}Ag_2SO_{4(hexagon)} \quad (6)$$

Table 2
Element composition measurements by EDS.

Spectrum	Element content (wt.%)				Total
	Ag	Ho	S	O	
Spectrum 1	23.22	35.49	13.78	27.51	100
Spectrum 2	23.19	35.49	13.80	27.52	100
Spectrum 3	23.20	35.50	13.78	27.52	100
Spectrum 4	23.19	35.46	13.80	27.55	100
Mean	23.20	35.49	13.79	27.52	100
Theory	23.20	35.48	13.79	27.53	100

The exothermic peak B at 604 °C is not accompanied by a change in mass, and its origin is interpreted by the interaction of simple sulfates with a new complex sulfate $AgHo(SO_4)_2$:

$$Ag_2SO_4 + Ho_2(SO_4)_3 \rightarrow 2AgHo(SO_4)_2 \quad (7)$$

The peak group C is attributed to the thermal decomposition of the double sulfate $AgHo(SO_4)_2$. The destruction of the compound takes place over a wide temperature range of 816.3–1093.4 °C. According to the TG data, it is possible to compile the overall equation of the process:

$$2AgHo(SO_4)_2 \rightarrow 2Ag + Ho_2O_2SO_4 + 3SO_2 + 2O_2 \quad (8)$$

According to the DSC data, the process proceeds in several stages. Obviously, in the first stage, the decay proceeds according to the equation:

$$2AgHo(SO_4)_2 \rightarrow 2Ag + Ho_2(SO_4)_3 + SO_2 + O_2 \quad (9)$$

Then, thermal destruction of the formed holmium sulfate $Ho_2(SO_4)_3$ is connected to this process, even before it is completed:

$$Ho_2(SO_4)_3 \rightarrow Ho_2O_2SO_4 + 2SO_2 + O_2 \quad (10)$$

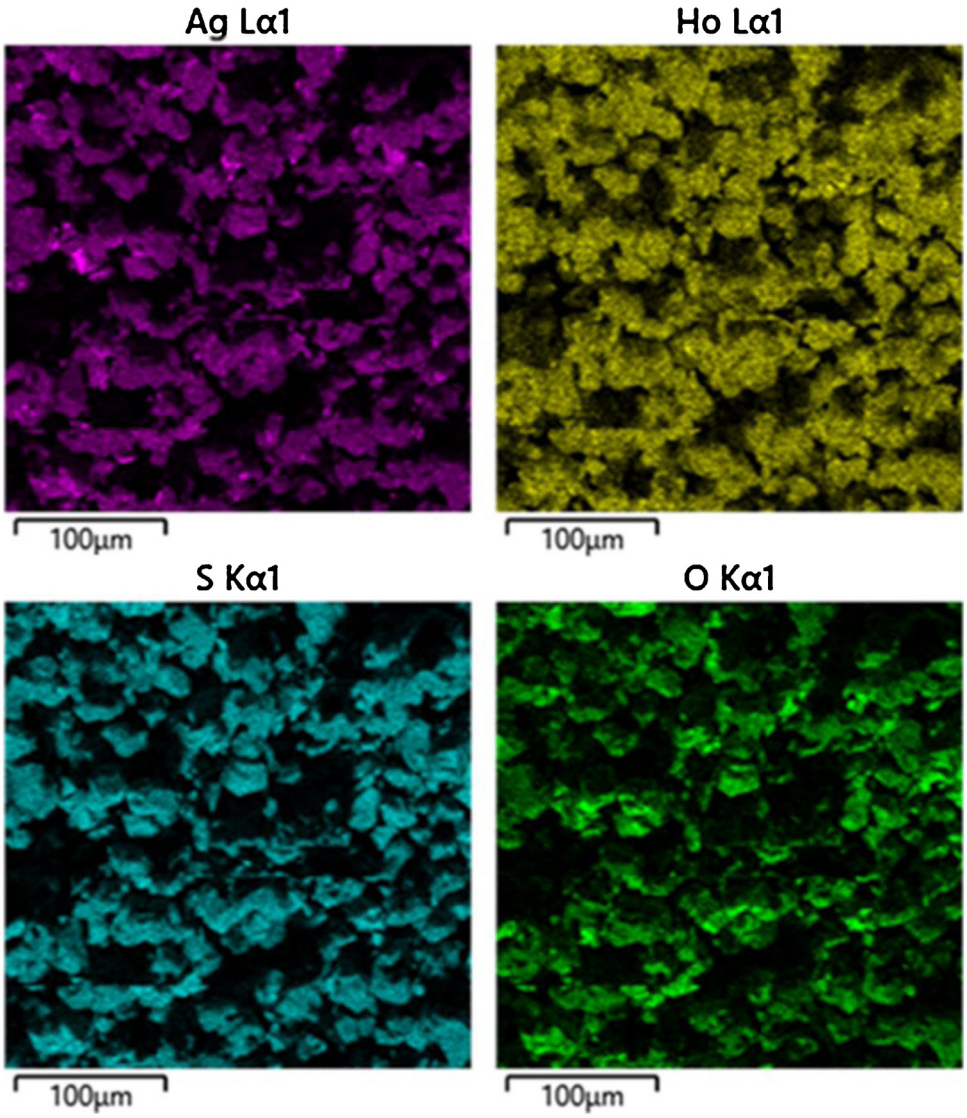

Fig. 6. Maps of the constituent element distribution in the powder sample of $AgHo(SO_4)_2$.

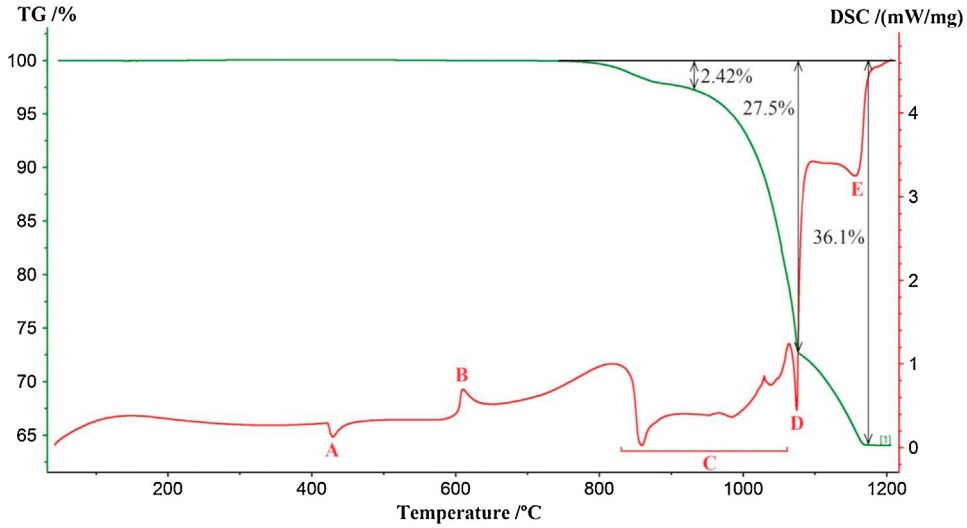

Fig. 7. TG/DSC curves recorded for the mixture of sulfates Ag_2SO_4 and $Ho_2(SO_4)_3$.

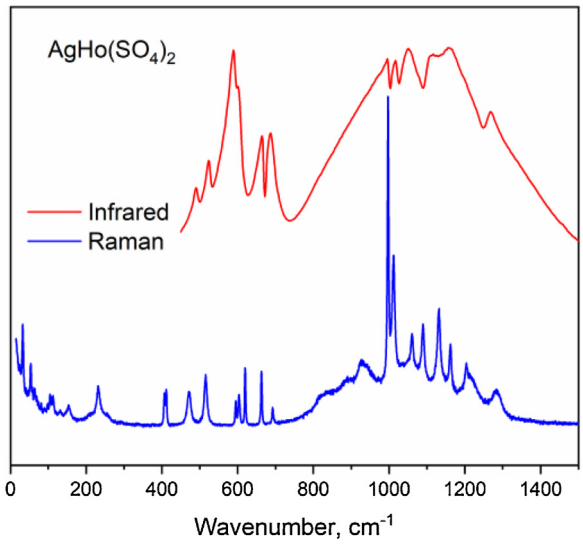

Fig. 8. Panoramic infrared and Raman spectra of $AgHo(SO_4)_2$.

Table 3
Correlation diagram between T_d point symmetry, C_s sites symmetry and C_{2h} factor group symmetry for SO_4 tetrahedra.

Wavenumber (cm^{-1}) [53]	T_d Point group	C_s Site symmetry	C_{2h} Factor group symmetry
983	A_1 (ν_1)	A'	A_g+B_u
450	E (ν_2)	A'+A"	$A_g+B_u+B_g+A_u$
1105	F_2 (ν_3)	2A'+A"	$2A_g+2B_u+B_g+A_u$
611	F_2 (ν_4)	2A'+A"	$2A_g+2B_u+B_g+A_u$

The peak D corresponds to the metallic silver melting process according to the literatures [51,52] and peak E corresponds to the holmium oxysulfate decomposition process:

$$Ho_2O_2SO_4 \rightarrow Ho_2O_3 + SO_2 + {}^1/_2O_2 \quad (11)$$

The infrared and Raman spectra of $AgHo(SO_4)_2$ are shown in Fig. 8. The vibrational representation for the monoclinic phase at the Brillouin zone center is: $\Gamma_{vibr} = 22A_g + 14B_g + 14A_u + 22B_u$ where acoustic modes are $\Gamma_{acoustic} = A_u + 2B_u$, and the remaining modes are optical ones. The Raman active modes are labeled as *g*-modes, and the infrared active modes are labeled as *u*-modes. The correlation diagram of internal vibrations between the free $[SO_4]^{2-}$ ions with the T_d symmetry, its site symmetry (C_s) and factor group symmetry (C_{2h}) of the unit cell [53] is given in Table 3. Taking into account that $AgHo(SO_4)_2$ has two crystallographically independent SO_4 tetrahedra, it can be concluded that eight vibrational modes appear in the range of stretching vibrations, two of them are symmetric stretching and six are antisymmetric stretching modes. Two sharp high intensity peaks were assigned to symmetric stretching vibration of SO_4 tetrahedra, the sharp medium intensity peaks related to the antisymmetric stretching of SO_4 and the remain broad bands were characterized as luminescent ones. The appearance of holmium luminescence bands in the high frequency region of Raman spectra (Fig. S4 in Supporting Information) is related to using the 514.5 Ar^+ laser as the excitation source. According to the group theoretical analysis, the Raman spectrum in the region of ν_4 vibrations of SO_4 tetrahedra (580 and 720 cm^{-1}) should consist of six lines (Table 3), and a complex band in the range of 390–530 cm^{-1} (region of ν_2 vibrations of SO_4 tetrahedra) should contain four lines, but only three of them are clearly seen in the experimental spectrum due to the overlapping of spectral bands (Fig. S5 in Supporting Information). The stretching modes

Table 4
Calculated (Raman) wavenumbers versus experimental Raman and IR data.

Raman exp. (cm^{-1})	Raman calc. (cm^{-1})	Infrared exp. (cm^{-1})	Assignment
1162	1168	1269	
1131	1120	1161	ν_3 SO_4
1089	1089	1111	
1061		1049	
1012	1004	1016	ν_1 SO_4
997		995	ν_1 SO_4
692	699	687	
662	674	663	
620	631	601	ν_4 SO_4
606	605		
603	576		
594		589	
515	539	532	
471	497	489	ν_2 SO_4
411	386		
406	372		
	352		
252	299		
232	226		rot. SO_4
209			
154			
132			
113			
105			
65			
54			
32			

of $[SO_4]^{2-}$ ions in the infrared spectra are located between 950 and 1300 cm^{-1}. According to Table 3, two bands associated with symmetric stretching vibrations should be observed. In the case of infrared spectra, the symmetric stretching vibrations are antisymmetric through the cell. The part of the experimental IR spectrum below 735 cm^{-1} refers to the bending vibrations of SO_4 tetrahedra. The wavenumber values of Raman and IR modes in $AgHo(SO_4)_2$ are summarized in Table 4.

The overall high resolution visible range luminescence spectrum of $AgHo(SO_4)_2$ excited at 457.9 nm is shown in Fig. 9 in comparison with those from two reference crystals (trigonal holmium aluminum huntite $HoAl_3(BO_3)_4$ excited at the same wavelength [18] and monoclinic elpasolite Rb_2KHoF_6 excited at 355 nm [54]). The excitation at 457.5 nm populates the $^5G_6$ + $^5F_1$ states of holmium ion; however, the luminescence from these states back to the ground state $^5I_8$ in $AgHo(SO_4)_2$ is very weak and is not practically observed. Therefore, the population of terminating levels at the excitation transition is efficiently transferred to lower-lying states via radiative/radiationless relaxation. Three luminescent bands in the visible wavelength range at the transitions from different excited states to the ground state were detected from $AgHo(SO_4)_2$, namely, from $^5F_2$ + $^3K_8$ (centered at 489 nm), $^5S_2$ + $^5F_4$ (545 nm), and $^5F_5$ (654 nm). Additionally, a weak emission, peaking at 752 nm, at the transition between excited states $^5G_6$ + $^5F_1$ and $^5I_6$ was detected. The latter means that the branching coefficient from $^5G_6$ or $^5F_1$ to $^5I_6$ dominates over that to $^5I_8$. The strongest luminescent band of holmium ion in $AgHo(SO_4)_2$ is at the $^5S_2$ + $^5F_4$ to $^5I_8$ transition, while the $^5F_5$ to $^5I_8$ transition is roughly two times less intense. This situation is an intermediate one between two reference crystals, the spectra of which are presented in Fig. 9 for comparison. Namely, in huntite-structured $HoAl_3(BO_3)_4$, the luminescence from $^5F_5$ to $^5I_8$ strongly dominates over that from $^5S_2$ + $^5F_4$ to $^5I_8$. The Judd-Ofelt analysis and the rate-equation calculations performed for $HoAl_3(BO_3)_4$ indicate that the domination of $^5F_5$ emission is somehow explainable by the radiative decay only, but a much better agreement in luminescent band intensities was obtained with the account for the radiationless decay governed by a high vibrational frequency cutoff in that borate crystal.

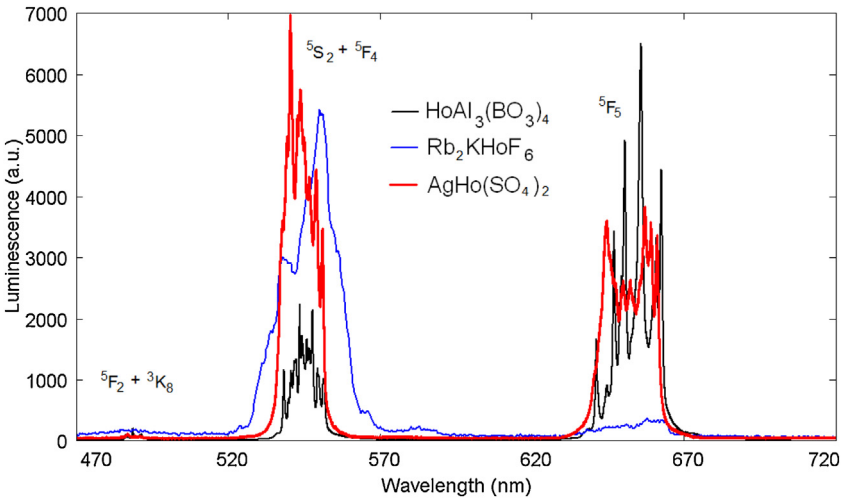

Fig. 9. Visible wavelength range of high resolution luminescence spectra of $AgHo(SO_4)_2$ (red, excited at 457.9 nm) and of reference crystals Rb_2KHoF_6 (blue, excited at 355 nm) and $HoAl_3(BO_3)_4$ (black, excited at 457.9 nm).

Fluoride crystals with a much lower vibrational frequency cutoff, like elpasolite Rb_2KHoF_6, in contrast to $HoAl_3(BO_3)_4$, exhibit the complete domination of $^5S_2$ + $^5F_4$ to the $^5I_8$ luminescence that must be treated as a sequence of both the variation of radiative probabilities and the decrease in the probability of radiationless decay, with the prevalence of the latter. The crystal under study, $AgHo(SO_4)_2$, is featured by higher vibrational frequencies closer to the borate one rather than the fluoride one. Therefore, the luminescent band intensity redistribution must be explained by the noticeable variation of Judd-Ofelt parameters in the crystal structure of $AgHo(SO_4)_2$ with respect to those in $HoAl_3(BO_3)_4$ rather than by the variation of radiationless transition probabilities. A more thorough analysis can be done after the measurements with oriented samples of the new crystal. Another interesting feature of the spectra in Fig. 9 is the shape of luminescent bands. Specifically, in $HoAl_3(BO_3)_4$, the individual lines corresponding to the transitions between crystal-field-split irreps of the corresponding energy levels are the narrowest, indicating a weak role of the interaction of electronic excitations with the vibrations of HoO_6 polyhedra. Oppositely, in fluorides, the quoted interaction plays the dominant role in the formation of the spectral shape of luminescent band to completely cover individual zero-phonon lines and shift the peak of the main luminescent band to the anti-Stokes side at room temperature. The spectral shapes of luminescent bands in $AgHo(SO_4)_2$ demonstrate the intermediate case, being closer to $HoAl_3(BO_3)_4$ than the fluoride. Individual lines within $AgHo(SO_4)_2$ spectral bands are still distinguishable but noticeably broadened with respect to the borate reference crystal, indicating a stronger interaction of electronic excitation with local vibrations.

More detailed picture of the influence of lattice dynamics on the shape of luminescent bands is shown in Figs. S6 and S7 (in Supporting Information), where the shapes of individual bands are compared at room temperature and at 77 K. The structure of bands at room temperature is kept but the upraise of shorter-wavelength part of the bands at room temperature with respect to the low-temperature spectra due to anti-Stokes emission with the absorption of thermal phonons is evident.

In order to explain the characteristics of electronic structure, the electronic band structure of $AgHo(SO_4)_2$ at 303 K were calculated based on the density functional theory (DFT). As holmium is one of lanthanide elements, the band structure is displayed as spin up and spin down band structures. As shown in Fig. 10, $AgHo(SO_4)_2$ belongs to compounds with indirect band gaps, and the valence band maximum (VBM) and conduction band minimum (CBM) are located at E and G points, while the spin up and spin down band gaps are 3.5 and 3.48 eV, respectively.

The total and spin-resolved partial densities of states (PDOS) are shown in Fig. 11 as calculated by DFT. Just as shown in the plots, the PDOS of Ag, S and O atoms do not display an obvious significant spin-splitting, while the two spin states of Ho atoms have strongly different PDOS patterns due to the spin-exchange interaction of the *f*-orbitals. Therefore, some tips should be promoted: (i) in the deep valence band (from−12 to−8 eV), the electron states mainly consist of Ho 4*f* spin up electrons, indicating that holmium atoms are difficult to overlap with other orbitals to form chemical bonds with high spin states; (ii) the electron level projections from −8 to −5 eV are dominantly occupied by S 3*p* and O 2*p* orbitals, which means that the sulfur atom hybridization with oxygen atoms forms $[SO_4]$ polyhedrons; (iii) the VBM top is composed of Ag 4*d*, Ho 4*f* spin down and O 2*d* orbitals, which implies that the hybridization occurred between Ag, Ho and O atoms; (iv) the Ho 4*f* spin down orbitals are strongly located at the bottom of CBM, indicating that the band gap is mainly governed by high-spin holmium atoms.

The first-principles lattice vibration analysis was performed to throw light on the microscopic mechanism of negative thermal expansion (NTE) in $AgHo(SO_4)_2$. According to the classical lattice dynamical theory, only lattice vibration phonons with the energy ($\hbar\,\omega$) lower than the elemental excitation of temperature (K_BT) could be excited under finite temperature (T) [55]. Thus, tracking the vibrational phonon assigned to the real space with respect frequency (ω) is an ineffective tunnel to unravel the microscopic mechanism of anomalous thermal expansion behavior. The maximum temperature of the observed negative thermal expansion is 703 K, corresponding to 491 cm^{-1}. This indicates that only the phonons below 491 cm^{-1} would dominantly contribute to the thermal expansion (as displayed in Fig. 12). It is revealed that these modes include two types of vibrations: orthogonal and parallel to the *b*-axis (especially S1-O1 bonds), as shown in Fig. S8 (in Supporting Information). The vibration parallel to the *b*-axis is suggestive of the symmetrical characteristic, which results in the balanced position, and it would not cause a change of the *b*-axis length. $AgHo(SO_4)_2$ is composed of $[HoO_8]$ and $[SO_4]$ polyhedrons to generate a three-dimensional network structure. The vibration along the *b*-axis is mainly related to the transversal vibration of the bridged oxygen atoms between these quasi-rigid $[HoO_8]$ and $[SO_4]$ polyhedrons. According to the "rigid unit model", the strengthening of these modes by increasing temperature would arouse the closing

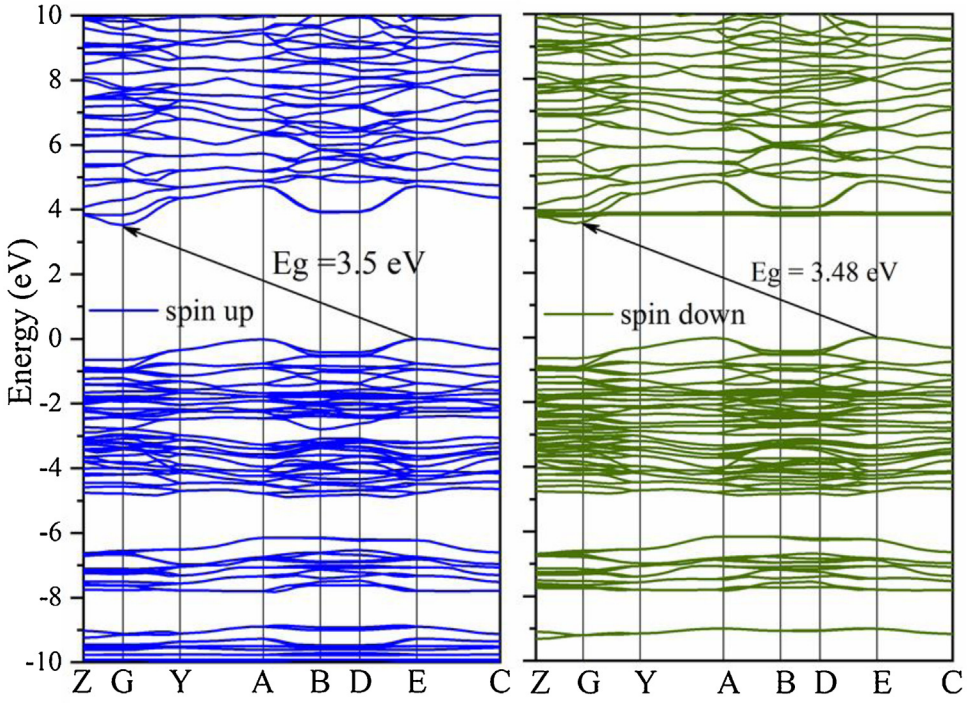

Fig. 10. $AgHo(SO_4)_2$ band structure: (a) for the spin up and (b) for the spin down.

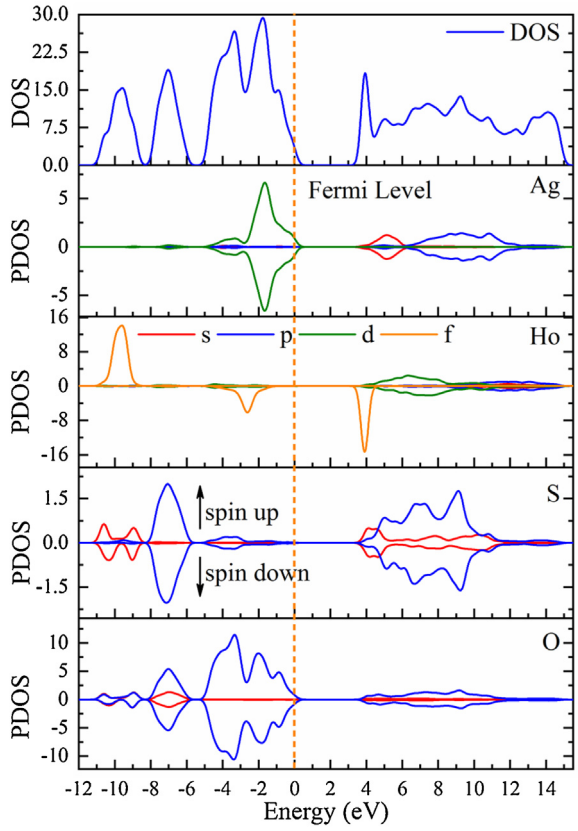

Fig. 11. Density of states of $AgHo(SO_4)_2$.

between the center atoms within the polyhedrons, which results in the contraction along the *b*-axis. Therefore, the net effect of all these modes is the negative thermal expansion behavior along the *b*-axis.

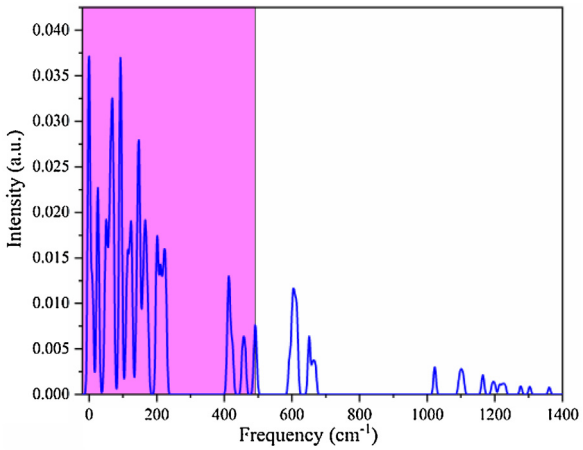

Fig. 12. $AgHo(SO_4)_2$ phonon DOS.

5. Conclusion

In the present work, the structural, thermal and luminescence spectral properties of new silver-holmium double sulfate were studied. It was established that the compound is formed as a result of the solid-phase reaction between simple sulfates at 604 °C and is stable up to 800 °C. The thermophysical measurements carried out in the temperature range of 143–703 K indicated the unusual behavior of the $AgHo(SO_4)_2$ crystal. Heating the sample leads to a decrease in cell parameter *b* and a simultaneous increase in cell parameters *a* and *c*. This effect was first observed in complex sulfates. It should be mentioned that triclinic $AgEu(SO_4)_2$ previously studied was characterized by an increase in all cell parameters upon heating. It can be reasonably assumed that strongly anisotropic thermal expansion is a specific characteristic of monoclinic sulfates $AgLn(SO_4)_2$. Besides, $AgHo(SO_4)_2$ exhibits sufficiently effective luminescent properties which are characteristic for compounds containing Ho^{3+} ions. Thus, the new double holmium-silver sulfate

is a promising multifunctional material. A further study of the class of $AgLn(SO_4)_2$ compounds and solid solutions based on them is of current interest in order to find the phases of the zero-value thermal expansion coefficient in a certain crystallographic direction.

Acknowledgements

This work was financially supported by the Russian Foundation for Basic Research (Nos. 18-02-00754 and 18-32-20011), the National Scientific Foundations of China (No. 11974360) and the Russian Science Foundation (No. 19-42-02003, in the part of conceptualization). M.S. Molokeev, A.S. Aleksandrovsky, A.S. Krylov, and A.S. Oreshonkov are grateful to Basic Project of the Ministry of Science of the Russian Federation in part of XRD, luminescent and Raman studies. IR-spectrometry was performed using resources of the Research Resource Center Ñatural Resource Management and Physico-Chemical Research: Use of equipment of Krasnoyarsk Regional Center of Research Equipment of Federal Research Center «Krasnoyarsk Science Center SB RAS» is acknowledged.

Appendix A. Supplementary data

Supplementary material related to this article can be found, in the online version, at doi:https://doi.org/10.1016/j.jmst.2020.10.026.

References

[1] D. Alezi, Y. Belmabkhout, M. Suyetin, P.M. Bhatt, Łukasz J. Weseliński, V. Solovyeva, K. Adil, I. Spanopoulos, P.N. Trikalitis, A.H. Emwas, M. Eddaoudi, J. Am. Chem. Soc. 137 (2015) 13308–13318.
[2] C. Artini, J. Eur. Ceram. Soc. 37 (2017) 427–440.
[3] G. Akopov, M.T. Yeung, R.B. Kaner,Adv. Mater. 29 (2017), 1604506.
[4] S.S. Fedotov, N.A. Kabanova, A.A. Kabanov, V.A. Blatov, N.R. Khasanova, E.V. Antipov, Solid State Ion. 314 (2018) 129–140.
[5] J. Perles, C. Fortes-Revilla, E. Guttérrez-Puebla, M. Iglesias, M.A. Monge, C. Ruiz-Valero, N. Snejko, Chem. Mater. 17 (2005) 2701–2706.
[6] M. Kul, Y. Topkaya, I. Karakaya, Hydrometallurgy 93 (2008) 129–135.
[7] S.J. Mills, V. Petříček, A.R. Kampf, R. Herbst-Imer, M. Raudsepp, J. Solid State Chem. 184 (2011) 2322–2328.
[8] N.N. Golovnev, M.S. Molokeev, S.N. Vereshchagin, V.V. Atuchin, J. Coord. Chem. 68 (2015) 1865–1877.
[9] O.V. Andreev, Yu.G. Denisenko, E.I. Sal'nikova, N.A. Khritokhin, K.S. Zyryanova, Russ. J. Inorg. Chem. 61 (2016) 296–301.
[10] X.J. Wang, J.G. Li, M.S. Molokeev, Q. Zhu, X.D. Li, X.D. Sun, Chem. Eng. J. 302 (2016) 577–586.
[11] S.A. Osseni, Y.G. Denisenko, J.K. Fatombi, E.I. Sal'nikova, O.V. Andreev, J. Nanostruct. Chem. 7 (2017) 337–343.
[12] Y.G. Denisenko, V.V. Atuchin, M.S. Molokeev, A.S. Aleksandrovsky, A.S. Krylov, A.S. Oreshonkov, S.S. Volkova, O.V. Andreev, Inorg. Chem. 57 (2018) 13279–13288.
[13] Y.G. Denisenko, A.S. Aleksandrovsky, V.V. Atuchin, A.S. Krylov, M.S. Molokeev, A.S. Oreshonkov, N.P. Shestakov, O.V. Andreev, J. Ind. Eng. Chem. 68 (2018) 109–116.
[14] L. Zhang, F. Ma, Q.M. Guan, C. Wang, J. Alloys Compd. 802 (2019) 173–180.
[15] Y.G. Denisenko, M.S. Molokeev, A.S. Krylov, A.S. Aleksandrovsky, A.S. Oreshonkov, V.V. Atuchin, N.O. Azarapin, P.E. Plyusnin, E.I. Sal'nikova, O.V. Andreev, J. Ind. Eng. Chem. 79 (2019) 62–70.
[16] M.S. Wickleder, Chem. Rev. 102 (2002) 2011–2087.
[17] L. Feng, J. Wang, G. Tang, L.F. Liang, H.B. Liang, Q. Su, J. Lumin. 124 (2007) 187–194.
[18] D.A. Ikonnikov, A.V. Malakhovskii, A.L. Sukhachev, V.L. Temerov, A.S. Krylov, A.F. Bovina, A.S. Aleksandrovsky, Opt. Mater. 37 (2014) 257–261.
[19] P. Li, A. Ruehl, U. Grosse-Wortmann, I. Hartl, Opt. Lett. 39 (2014) 6859–6862.
[20] A.L. Sukhachev, A.V. Malakhovskii, A.S. Aleksandrovsky, I.A. Gudim, V.L. Temerov, Opt. Mater. 83 (2018) 87–92.
[21] P. Kronenberg, O. Traxer, World J. Urol. 33 (2015) 463–469.
[22] C. Netsch, B. Becker, C. Tiburtius, C. Moritz, A.V. Becci, T.R.W. Herrmann, A.J. Gross, World J. Urol. 35 (2017) 1913–1921.
[23] D.A. Wollin, A. Ackerman, C. Yang, T. Chen, Urology 103 (2017) 47–51.
[24] C.S. Lim, A. Aleksandrovsky, M. Molokeev, A. Oreshonkov, V. Atuchin, Phys. Chem. Chem. Phys. 17 (2015) 19278–19287.
[25] J. Zhang, Z.H. Hua, F. Zhang, Ceram. Int. 41 (2015) 9910–9915.
[26] C.S. Lim, V.V. Atuchin, A.S. Aleksandrovsky, M.S. Molokeev, Mater. Lett. 181 (2016) 38–41.
[27] D. Kasprowicz, P. Głuchowski, B.M. Maciejewska, M. Chrunik, A. Majchrowski, New J. Chem. 41 (2017) 9847–9856.
[28] C.S. Lim, V.V. Atuchin, A.S. Aleksandrovsky, M.S. Molokeev, A.S. Oreshonkov, J. Alloys Compd. 695 (2017) 737–746.
[29] S.J. Clark, M.D. Segall, C.J. Pickard, P.J. Hasnip, M.J. Probert, K. Refson, M.C. Payne, Z. Kristallogr. 220 (2005) 567–570.
[30] W. Kohn, L.J. Sham, Phys. Rev. 140 (1965) 1133–1138.
[31] M.C. Payne, M.P. Teter, D.C. Allan, T.A. Arias, J.D. Joannopoulos, Rev. Mod. Phys. 64 (1992) 1045–1097.
[32] J.P. Perdew, K. Burke, Phys. Rev. Lett. 77 (1996) 3865–3868.
[33] J.P. Perdew, Y. Wang, Phys. Rev. B 45 (1992) 13244–13249.
[34] D.R. Hamann, M. Schlüter, C. Chiang, Phys. Rev. Lett. 43 (1979) 1494–1497.
[35] H.J. Monkhorst, J.D. Pack, Phys. Rev. B 13 (1976) 5188–5192.
[36] M. Cococcioni, S. de Gironcoli,Phys. Rev. B 71 (2005), 035105.
[37] V.I. Anisimov, J. Zaanen, O.K. Andersen, Phys. Rev. B 44 (1991) 943–954.
[38] A.X.S. Bruker, TOPAS V4: General Profile and Structure Analysis Software for Powder Diffraction Data–User's Manual, Bruker A.X.S., Karlsruhe, Germany, 2008.
[39] V. Favre-Nicolin, R. Cerny, Mater. Sci. Forum 443-444 (2004) 35–38.
[40] V. Favre-Nicolin, R. Černý, J. Appl. Crystallogr. 35 (2002) 734–743.
[41] A.L. Spek, J. Appl. Crystallogr. 36 (2003) 7–13.
[42] A. Trzesowska, R. Kruszynski, T.J. Bartczak, Acta Crystallogr. B 60 (2004) 174–178.
[43] I.D. Brown, D. Altermatt, Acta Crystallogr. B 41 (1985) 244–247.
[44] A.W. Addison, T.N. Rao, J. Reedijk, J. van Rijn, G.C. Verschoor, J. Chem. Soc. Dalton Trans. 7 (1984) 1349–1356.
[45] V.A. Blatov, A.P. Shevchenko, D.M. Proserpio, Cryst. Growth Des. 14 (2014) 3576–3586.
[46] M.J. Cliffe, A.L. Goodwin, J. Appl. Crystallogr. 45 (2012) 1321–1329.
[47] R.A. Secco, E.A. Secco, Phys. Rev. B 56 (1997) 3099–3104.
[48] C.W.F.T. Pistorius, J. Chem. Phys. 46 (1967) 2167–2171.
[49] S.R. Rao, C.B. Lingam, D. Rajesh, R.P. Vijayalakshmil, C.S. Sunandana, IOSR J. Appl. Phys. 4 (2013) 39–43.
[50] H.B. Larsen, G. Thorkildsen, D.G. Nicholson, P. Pattison, Cryst. Res. Technol. 51 (2016) 730–737.
[51] J.K. Johnstone, J. Electrochem. Soc. 112 (1965) 25C–27C.
[52] D.M. Speros, R.L. Woodhouse, J. Phys. Chem. 67 (1963) 2164–2168.
[53] K. Nakamoto, Infrared and Raman Spectra of Inorganic and Coordination Compounds, 6th ed., Wiley, New York, 2009.
[54] A.S. Aleksandrovsky, A.S. Krylov, A.V. Malakhovskii, V.N. Voronov, J. Lumin. 132 (2012) 690–692.
[55] P.Y. Long, H. Tong, X.S. Miao,Appl. Phys. Express 5 (2012), 031201.